Acknowledgments

This work was supported by the "863" project (# 2003AA302640) of MST and Postdoctoral Funding (# 20040055020) of Ministry of Education, China.

References

[1] Liu C, Cheng HM, Cong HT, Li F, Su G, Zhou BL, et al. Synthesis of macroscopically long ropes of well-aligned single-walled carbon nanotubes. Adv Mater 2000;12(16):1190–2.
[2] Nikolaev P, Bronikowski M, Bradley RK, Rohmund F, Colbert DT, Smith KA, et al. Gas-phase catalytic growth of single-walled carbon nanotubes from carbon monooxide. Chem Phys Lett 1999;313(1–2): 91–7.
[3] Hata K, Futaba DN, Mizuno K, Namai T, Yumura M, Iijima S. Water-assisted highly efficient synthesis of impurity-free single-walled carbon nanotubes. Science 2004;306(5700):1362–4.
[4] Itkis ME, Perea DE, Niyogi S, Love J, Tang J, Yu A, et al. Optimization of the Ni–Y catalyst composition in bulk electric arc synthesis of single-walled carbon nanotubes by use of near-infrared spectroscopy. J Phys Chem B 2004;108(34):12770–5.
[5] Kong J, Soh HT, Cassell AM, Quate CF, Dai HJ. Synthesis of individual single-walled carbon nanotubes on patterned silicon wafers. Nature 1998;395(6705):878–81.
[6] Cheung CL, Kurtz A, Park H, Lieber CM. Diameter-controlled synthesis of carbon nanotubes. J Phys Chem B 2002;106(10): 2429–33.
[7] Landi BJ, Ruf HJ, Evans CM, Cress CD, Raffaelle RP. Purity assessment of single-wall carbon nanotubes, using optical absorption spectroscopy. J Phys Chem B 2005;109(20):9952–65.
[8] Lv X, Du F, Ma YF, Wu Q, Chen YS. Synthesis of high quality single-walled carbon nanotubes at large scale by electric arc using metal compounds. Carbon 2005;43(9):2020–2.
[9] Gorbunov A, Jost O, Pompe W, Graff A. Solid-liquid-solid growth mechanism of single-wall carbon nanotubes. Carbon 2002;40(1): 113–8.
[10] Rao AM, Chen J, Richter E, Schlecht U, Eklund PC, Haddon RC, et al. Effect of van der Waals interactions on the raman modes in single walled carbon nanotubes. Phys Rev Lett 2001;86(17): 3895–8.

The effect of cooling rate on hydrogen release from a pyrolytic carbon coating and its resulting morphology

Boris Reznik [a,*], Koyo Norinaga [b], Dagmar Gerthsen [a], Olaf Deutschmann [b]

[a] *Laboratory for Electron Microscopy, University of Karlsruhe, 76128 Karlsruhe, Germany*
[b] *Institute for Chemical Technology and Polymer Chemistry, University of Karlsruhe, 76128 Karlsruhe, Germany*

Received 15 September 2005; accepted 7 December 2005
Available online 6 January 2006

Keywords: Porous carbon; Pyrolytic carbon; Scanning electron microscopy; Chromatography

The formation mechanism of deposits of pyrolytic carbon is a complex process involving homogeneous reactions in the gas phase, heterogeneous reactions at the substrate surface and subsequent dehydrogenation. All three processes are relevant for the final carbon structure and other physical properties [1,2]. Many studies are devoted to the analysis of the products of the hydrocarbon pyrolysis [1–4]. However, up to now experimental results demonstrating directly the dehydrogenation process have not yet been presented. Presumably the dehydrogenation process can be controlled by the thermal treatment of the deposit after the termination of the deposition, e.g. by the reactor cooling rate. In the present work, we study the effect of cooling rate on the release of hydrogen from a pyrolytic carbon coating and its resulting morphology.

Pyrolytic carbon coatings were deposited onto monolithic cordierite substrates placed in a vertical flow hot wall reactor by using ethene with a purity of better than 99.4% as the hydrocarbon precursor. The hot wall reactor used in this study is identical with the reactor described in a previous study [5]. Briefly, the deposition space is formed by a cylindrically shaped alumina tube with a diameter of 22 mm and a length of 40 mm. The inlet and outlet tubes of the reactor (8 mm in diameter) are connected to the deposition space through conical inlet and outlet nozzles. A channel structure, made of cordierite, with 25 channels per square inch, i.e. 4.4×4.4 mm^2/channel, is fitted in the alumina tube, resulting in a surface area/volume ratio of the deposition space of $[A/V] = 0.9$ mm^{-1}. The deposition experiments were performed at 950 °C, 4 kPa ethene pressure, and a residence time of 1 s. After a deposition duration of 70 h, the supply of ethene was stopped and argon was supplied with a flow rate of 33 ml/min. The reactor was then cooled down to room temperature. To reveal

* Corresponding author.
E-mail address: reznik@lem.uni-karlsruhe.de (B. Reznik).

0008-6223/$ - see front matter
doi:10.1016/j.carbon.2005.12.014

the effect of the cooling rate, two different cooling rates were chosen: 300 and 6 °C/h achieved by using a temperature controller (EUROTHERM). During the cooling, the gaseous products were analyzed on-line with a gas chromatograph (Sichromat 3,Siemens) equipped with a vacuum dosing system and with a thermal conductivity detector. Three independent runs were performed to confirm the repeatability of the measurements. Prior to each run, the reactor was cleaned by heating the reactor under ambient conditions up to 950 °C to remove carbon deposited on the inner wall of the tube.

The morphology of pyrolytic carbon coatings can be studied by different microscopical methods such as light microscopy, atomic force microscopy or scanning electron microscopy (SEM). Among these techniques SEM combines two important features: sample preparation steps can be avoided and the morphological features can be imaged in a broad range of spatial levels ranging from some tens of nanometers to several hundred micrometers.

The coating morphology was characterized using a LEO 1530 Gemini scanning electron microscope (SEM) equipped with a Schottky field-emission gun. The coatings were observed without any kind of sample preparation to avoid preparation-induced artifacts. The coating morphology was investigated from two perspectives: parallel (surface) and perpendicular (cross-section view) with respect to the substrate surface. The area fraction of pits on the coating surface observed in SEM images was defined as the area covered by pits divided by the total surface area of the micrograph. For this purpose the total value of black pixels (pit area) related to the measured area of the micrograph was determined using the "analySIS" image analysis software (Soft-Imaging Software, Münster, Germany).

During the cooling experiments, oxygen and hydrocarbon compounds were not detected by gas chromatography. Only the peak corresponding to molecular hydrogen was observed for the studied samples.

Fig. 1 shows the variation of the reactor temperature and the total accumulated molecular hydrogen (H_2 release) amount as a function of time after chemical vapor deposition at different reactor cooling rates. For the rapid cooling rate of 300 °C/h hydrogen is released continuously for about 1 h (Fig. 1a and c). After 0.9 h, saturation takes place, corresponding to a total amount of released hydrogen of 0.06 mmol. In contrast, for the lower cooling rate of 6 °C/h, a larger amount of hydrogen of 0.9 mmol is accumulated (Fig. 1b and d). In this case hydrogen is released continuously up to 30 h (Fig. 1d). The release of the molecular hydrogen occurs within a certain temperature range between the deposition temperature and a lower limit between 600 and 800 °C (Fig. 1).

Fig. 2 shows SEM micrographs of the coatings cooled down with different rates. A cellular surface morphology is observed in both cases at the micrometric scale (Fig. 2a and c). In the case of the sample cooled at 300 °C/h (Fig. 2a), pits with a diameter up to 22 nm are observed at the nanometric scale (Fig. 2b). It is remarkable to note a relatively random pit location. For instance, there is no preferential pit appearance along the cell boundaries (Fig. 2b). The area fraction of pits on the surface is about 0.2%. An evident larger amount of pits is observed in deposits cooled down with 6 °C/h (Fig. 2d). The diameter

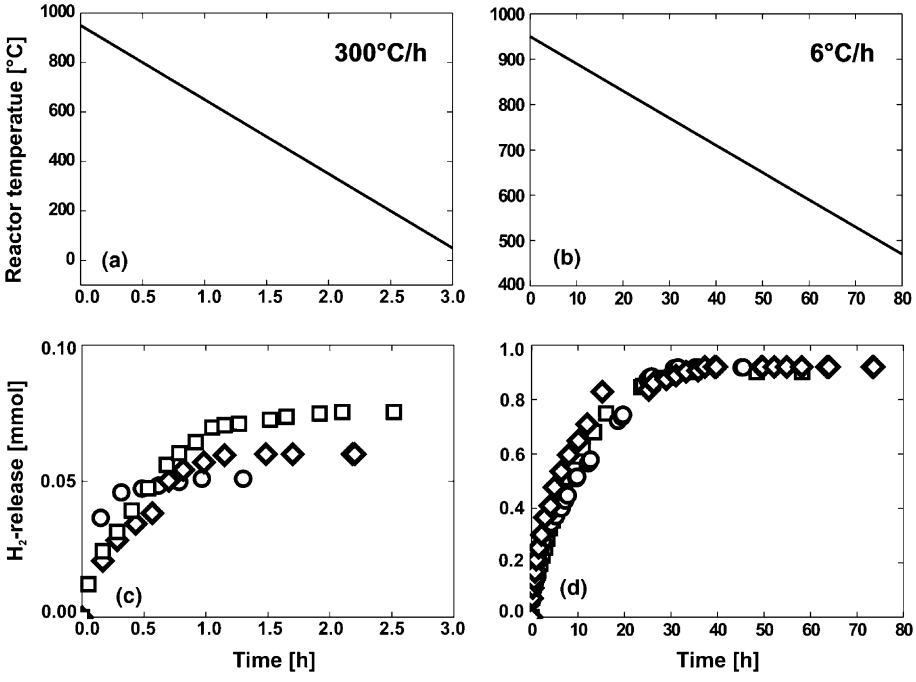

Fig. 1. Reactor temperature (a, b) and amount of released hydrogen (c, d) as a function of time at cooling rates of 300 °C/h (right-hand side figures) and 6 °C/h (left-hand side figures). The symbols in (c, d) mark three different runs.

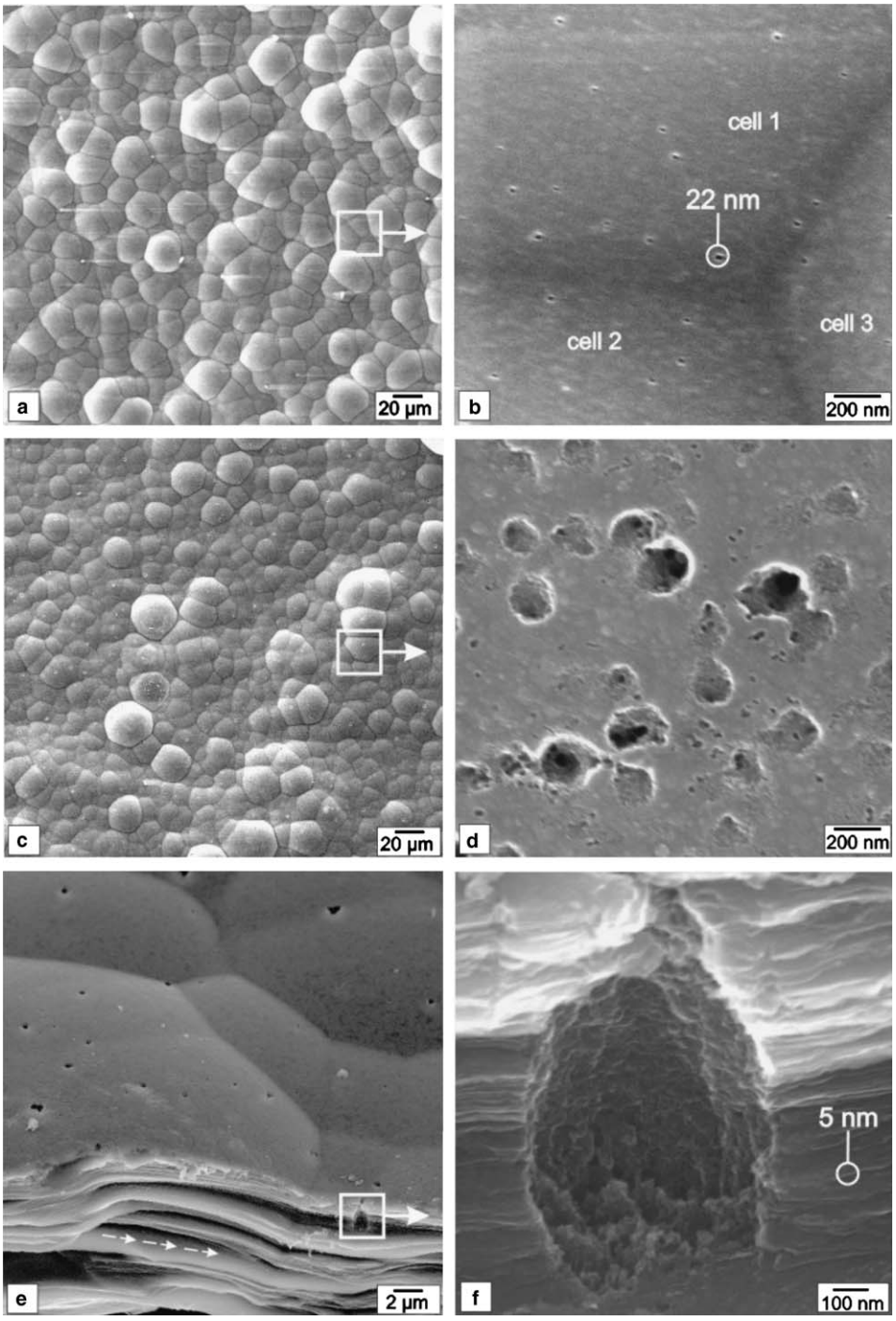

Fig. 2. Scanning electron micrographs of coatings cooled down with 300 °C/h (a, b) and 6 °C/h (c, d, e, f). (a, b, c, d)—surface images, (e, f)—cross-section images. Dashed arrows in (e) mark exfoliation parallel to the substrate surface (see text for details).

of pits ranges from about 20 up to 200 nm. The area fraction of pits is about 17%. No preferential pit location was observed as in the case of the fast cooling rate (Fig. 2d). Figs. 2e and f shows SEM micrographs of the coating cooled down with 6 °C/h in a cross-section view. The cross-section perspectives were obtained from cleaved as-produced material. The images demonstrate an extensive deposit exfoliation (see the dashed arrows in Fig. 2e). It is remarkable to note that pits do not extend through the whole coating thickness but are located within a surface region with a thickness of about 1.6 μm (Fig. 2e). An extensive eroded inner surface of the large pits is typical (Fig. 2f) while the surrounding coating is composed of well-developed planar piles oriented parallel to the substrate surface.

The major finding established in the current work is a clearly quantitative demonstration of the evidence of the

hydrogen release after low-temperature chemical vapor deposition (CVD). These results imply that the deposited pyrolytic carbon is not a pure carbon but a hydrocarbon material which is consistent with previous theoretical and experimental results [1–10]. The cracking of hydrocarbon precursor gases during low-temperature CVD is associated frequently with the formation of hydrogen-containing polymeric products at the substrate surface [1,2] such as viscous polymer-like droplets [8], a flat polymer film [9], a mesogenic liquid film [10]. Using elastic recoil detection analysis Lavenac et al. [4] found out that the hydrogen concentration lies between 1 and 4 at.%. An indirect presence of hydrogen-bonded carbon in pyrolytic carbon coatings is demonstrated by electron-energy-loss spectroscopy showing an energy shift and intensity fluctuation of plasmon peaks [6] or intensity and shape fluctuation of C K-shell peaks [7]. Recently, using force modulation in atomic force microscopy Pfrang et al. [11] observed a contrast variation in pyrolytic carbon coatings which can be interpreted in terms of an intermediate, non-pure carbon phase.

Considering the deposited material as a hydrocarbon or (hydrogen-containing) material, it is reasonable to suggest that pyrolysis continues after the deposition until temperatures between 600 and 800 °C (Fig. 1) are reached. During this temperature range hydrocarbon bond breaking occurs and the molecular hydrogen is released. A similar temperature-induced hydrogen release was reported by Orimo et al. [12] during the investigation of the hydrogen desorption properties of mechanically prepared nanostructured graphite.

At present, we cannot present a detailed explanation of the pit formation process. A rough idea can be given by considering that pits are located in the uppermost part of the coating. This part of the coating corresponds to the final deposition stage. The region in the vicinity of the surface is likely to contain a higher hydrogen concentration as compared to the lower parts of the coating, for which we expect hydrogen loss already during the deposition process. Consequently, such a ''soft'' material could be etched by the released hydrogen during the cooling phase. Similar pits were observed by Rodriguez-Reinoso and Thrower [13] in oxidized highly oriented pyrolytic graphites. It was also observed that the pits do not extend through the whole coating thickness.

For the first time, the effect of cooling rate on hydrogen release from a pyrolytic carbon coating and its resulting morphology has been studied by a combination of gas chromotography and scanning electron microscopy. The release of molecular hydrogen decreases strongly with increasing cooling rate. The release of the molecular hydrogen occurs at high temperature. It stops at a lower limit between 600 and 800 °C (Fig. 1). The increased hydrogen release correlates with an increased density of pits in the uppermost part of the pyrolytic carbon coating. The present data demonstrate the relevance of the dehydrogenation process after CVD implying a continuation of pyrolysis within the deposited hydrocarbon material. In addition to pressure, temperature, residence time and surface area/reactor volume ratio the cooling rate—or more generally the thermal history of the material—should be given when CVD processes are analyzed [1,2,5,11]. The thermal history after the deposition of pyrolytic carbon can also be used to control the microstructural properties of different materials derived from hydrocarbon gaseous sources such as pyrolytic carbon matrices of carbon/carbon composites, nanotubes and activated carbons.

Acknowledgements

The present study was performed in the ''Sonderforschungsbereich 551 ''Carbon from the gas phase: elementary reactions, structures, materials''. The financial support from the German Research Foundation (DFG) is gratefully acknowledged. The authors would like to thank K.J. Hüttinger, W. Send and M. Fotouhi for many fruitful discussions.

References

[1] Bokros JC. Deposition, structure, and properties of pyrolytic carbon. In: Walker PL, editor. Chemistry and physics of carbon, vol. 5. New York: Dekker; 1969. p. 1–118.
[2] Oberlin A. Pyrocarbons. Carbon 2002;40:7–24.
[3] Chen CJ, Back MH. The simultaneous measurement of the rate of formation of carbon and of hydrocarbon products in the pyrolysis of methane. Carbon 1979;17:175–80.
[4] Lavenac J, Langlais F, Bourrat X, Naslain R. Deposition process of laminar pyrocarbon from propane. J Phys IV Fr 2001;11:3-1015–21.
[5] Norinaga K, Hüttinger KJ. Kinetics of surface reactions in carbon deposition D from light hydrocarbons. Carbon 2003;41:1509–14.
[6] Reznik B, Fotouhi M, Gerthsen D. Structural analysis of pyrolytic carbon deposits on a planar cordierite substrate. Carbon 2004;42:1311–3.
[7] Reznik B, Gerthsen, Hüttinger KJ. Micro- and nanostructure of the carbon matrix of infiltrated carbon fiber felts. Carbon 2001;39:215–29.
[8] Shi R, Li HJ, Yang Z, Kang MK. Deposition mechanism of pyrolytic carbons at temperature between 800 and 1200 °C. Carbon 1997;35:789–92.
[9] Hirai T, Yajima S. Structural features of pyrolytic graphite. J Mater Sci 1966;2:18–27.
[10] Hu J, Hüttinger KJ. Mechanisms of carbon deposition—a kinetic approach. Carbon 2002;40:624–8.
[11] Pfrang A., Wan YZ, Schimmel Th. Direct observation of intermediate phases of pyrolytic carbon by atomic force microscopy. CD-ROM, An international conference on carbon, Gyeongju, Korea, 2005, Paper P10-01.
[12] Orimo A, Matsushima T, Fujii H. Hydrogen desorption property of mechanically prepared nanostructured graphite. J Appl Phys 2001;90:1545–9.
[13] Rodriguez-Reinoso F, Thrower P. Microscopic studies of oxidized highly oriented pyrolytic graphites. Carbon 1974;12:269–79.